International Journal of Green Energy

ISSN: (Print) (Online) Journal homepage: www.tandfonline.com/journals/ljge20

Modified reconstruction of boiler numerical temperature field based on flame image feature extraction

Jiajian Long, Meirong Dong, Jieheng Zhou, Youcai Liang & Jidong Lu

To cite this article: Jiajian Long, Meirong Dong, Jieheng Zhou, Youcai Liang & Jidong Lu (2024) Modified reconstruction of boiler numerical temperature field based on flame image feature extraction, International Journal of Green Energy, 21:14, 3173-3187, DOI: 10.1080/15435075.2024.2360455

To link to this article: https://doi.org/10.1080/15435075.2024.2360455

Published online: 02 Jun 2024.

INTERNATIONAL JOURNAL OF GREEN ENERGY
2024, VOL. 21, NO. 14, 3173–3187
https://doi.org/10.1080/15435075.2024.2360455

Modified reconstruction of boiler numerical temperature field based on flame image feature extraction

Jiajian Long[a,b], Meirong Dong[a,b], Jieheng Zhou[a,b], Youcai Liang[a,b], and Jidong Lu[a,b]

[a]School of Electric Power, South China University of Technology, Guangzhou, Guangdong, China; [b]Guangdong Province Engineering Research Center of High Efficient and Low Pollution Energy Conversion, Guangzhou, Guangdong, China

ABSTRACT

Computational fluid dynamics (CFD) method is a common method to obtain the temperature field distribution within the furnace. However, in order to reduce computational complexity, the numerical simulation involve simplifications in boundary conditions and model parameters. As a result, the temperature field distribution deviates from the actual operating conditions. This paper proposes a numerical temperature field modification method based on flame images. Flame images corresponding to the operational conditions are collected using the Industrial Flame Monitoring System (IFMS). The flame images are preprocessed, and the contour of the flame's core region is extracted using the Mask Region-based Convolutional Neural Network (Mask R-CNN) method. The geometric features of the flame are extracted, and matrix calculations are applied to modify the numerical temperature field. The modified temperature field exhibits a deviation in the combustion center, aligning with the actual operation of the boiler. A comparison between the modified temperature field and the temperature measurements from flue gas shows consistent temperature trends. The absolute error (AE) under different operating conditions is under 8.8 K, and the relative error (RE) remains below 1.3%. The analysis results demonstrate that it can enhance the accuracy of temperature field calculations by the modification from flame image features.

ARTICLE HISTORY
Received 16 February 2024
Accepted 22 May 2024

KEYWORDS
Flame images; feature extraction; CFD; numerical temperature field; modified reconstruction

1. Introduction

In the current development of energy forms, thermal power generation still holds a significant position. As the core equipment of coal-fired power plants, the operation of boilers directly impacts the overall performance of the units (Nemitallah et al. 2023; Shi et al. 2019; Strušnik et al. 2021; Wang et al. 2018). However, due to the high-temperature and high-dust atmosphere formed by the combustion of coal powder in the furnace, with the core temperature reaching around 1873.15K, a large amount of coal ash and slag is generated, making it difficult to monitor the real-time status parameters inside the furnace using conventional measurement points. To overcome the "black box" situation inside the furnace during boiler operation, various non-contact measurement methods have been developed. For example, temperature measurement using acoustic methods based on time-of-flight inversion calculations (Kong et al. 2020; Wu et al. 2021; Zhang, Shen, and An 2019), and temperature field reconstruction using optical inversion techniques (Blondeau et al. 2020; Lou and Zhang 2019; Mu et al. 2015). These methods require the installation of multiple sensing and receiving devices at different positions in the furnace, increasing the overall system complexity.

In recent years, with the significant development and application of artificial intelligence algorithms, many researchers have discussed combining Computational Fluid Dynamics (CFD) with intelligent algorithms to achieve rapid prediction of physical fields or related thermal distributions. This integration aims to meet the needs of diagnosis and optimization during online operation of boilers. Tang et al. (2023) and Lv et al. (2023) respectively employed Extreme Learning Machine (ELM) and Incremental Deep Extreme Learning Machine (IDELM) in conjunction with CFD numerical simulations to successfully predict the heat flux density and temperature distribution of boilers. Furthermore, there are studies that use dimensionality reduction techniques on CFD numerical results, using the reduced-dimensional results as inputs for reconstruction using intelligent algorithms. For example, combining Principal Component Analysis (PCA) for dimensionality reduction of CFD results and constructing a Convolutional Autoencoder for reconstruction of boiler temperature field distribution (Jiang et al. 2023; Sun et al. 2022). The CFD data source serves as the foundation for model construction, and the accuracy of the sample is critical for the prediction results.

In the case of tangential-fired boilers, CFD numerical simulations are generally based on the operational data from the boiler's Distributed Control System (DCS) to construct cases for different operating conditions. In CFD simulations, simplifications and assumptions are often made regarding boundary conditions, model parameters, and other factors to reduce computational complexity (Ali, Najim, and Rishack 2017; Belošević et al. 2019; Chen et al. 2019; Tan et al. 2018). However, in practical industrial applications, the combustion is often uneven due to the long-term abrasion and ash

CONTACT Meirong Dong epdongmr@scut.edu.cn School of Electric Power, South China University of Technology, Guangzhou, Guangdong 510640, China

accumulation of coal feed and air feed channels. This can result in the phenomenon of flame center deviation, causing the flame to lean toward one side of the tubes, leading to overheating and rupture. The simplifications and assumptions can result in discrepancies between the numerically obtained temperature field from CFD and the actual temperature distribution inside the boiler. Therefore, it is necessary to incorporate more operational information from the on-site boiler to modify the physical field distribution.

In thermal power boilers, Industrial Flame Monitoring System (IFMS) is equipped to monitor flame extinguishment and combustion stability, capturing videos of the flame combustion through cameras. These recorded flame video images contain a wealth of feature parameters related to flame combustion that can be extracted. Chen, Chan, and Cheng (2013) studied the extraction of combustion-related features from flame images and applied principal component analysis and Gaussian processes for the rapid prediction of flue gas outlet composition. Zhou et al. (2021) focused on the burner and constructed the Basis Image Monitor (BIM) model using Convolutional Neural Networks (CNN) to extract combustion features from flame shapes. This enabled the recognition of flame-wall interaction, attached flame, outer shear layer flame (OSL flame), and mixing effects during combustion. Wang et al. (2020) proposed a combustion diagnosis method based on image processing to identify abnormal conditions in gas flames. They specifically obtained flame contours through threshold segmentation and defined 12 typical features including flame area, rectangularity, connectivity, and circularity. Fuzzy recognition is then used for classification of different combustion states, achieving a prediction accuracy of over 90%. Ronquillo-Lomeli and García-Moreno (2024) utilized the Feature Subset Selection (FSS) algorithm to extract five flame indices related to combustion states, including flame color, flame length, flame intensity, aperture of flame shape, and density. They employed a Probabilistic Neural Network (PNN) for flame feature clustering and calculated flame indices to evaluate the combustion state of the burner, achieving an accuracy of 92.3%. In summary, the feature value of flame images can be exploited to obtain information related to combustion features. Exploring effective utilization of this image information holds great research prospects, particularly when applied to the study of combustion field distributions.

In this work, we propose a temperature field modification and reconstruction method based on flame image features. Firstly, the CFD method is utilized to obtain multiple sets of temperature field distributions for different operating conditions. Then, the flame images are processed to extract the high-temperature core flame contours by using Mask Region-based Convolutional Neural Network (Mask R-CNN). Afterword, the flame feature is extracted to form a modification matrix. By applying the matrix modification method, the CFD temperature field is modified and compared with the actual parameters to verify the accuracy and reliability. This further enhances the feasibility of applying the numerical temperature field in the real-time operation of boilers, thereby benefiting the improvement of on-site combustion diagnostic capability.

2. Methodology and materials

2.1. Research object

The research object in this work is a 330 MW tangentially-fired boiler. The detail information can be found our previous work (Ye et al. 2022). Briefly, the geometric dimensions of the boiler and its geometric model are presented in Figure 1. Based on the coal powder flow and combustion conditions, the research area is divided into the Burner region, Transitional region, and flame corner region. The combustion inside the furnace is concentrated in the Burner region, which consists of 16 numbered burner groups.

2.1.1. CFD model

The combustion of a tangentially-fired coal boiler involves various physical and chemical processes, including gas-phase turbulence, particle motion, volatile decomposition and combustion, char combustion, radiative heat transfer, and nitrogen

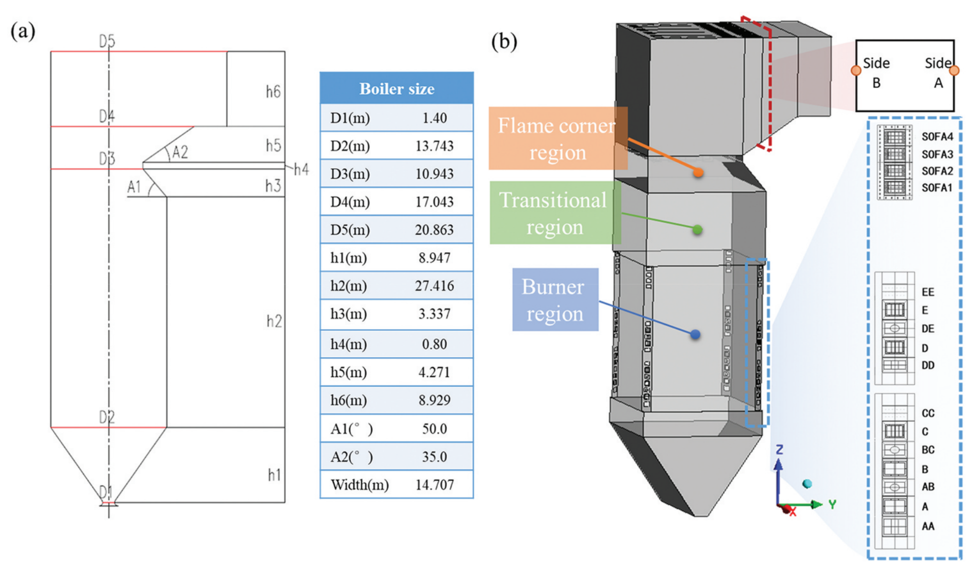

Boiler size	
D1(m)	1.40
D2(m)	13.743
D3(m)	10.943
D4(m)	17.043
D5(m)	20.863
h1(m)	8.947
h2(m)	27.416
h3(m)	3.337
h4(m)	0.80
h5(m)	4.271
h6(m)	8.929
A1(°)	50.0
A2(°)	35.0
Width(m)	14.707

Figure 1. Tangential boiler geometric modeling (a)Boiler size; (b)Boiler geometric model.

oxide formation. These processes are described and calculated using corresponding commonly used models, as shown in Table 1.

A mesh grid model is constructed based on the geometric model, as shown in Figure 2 (a). The burner area where intense turbulent combustion occurs in the furnace is locally refined to reduce numerical simulation artifacts and improve the accuracy of the results, as depicted in Figure 2(b). Grid independence tests are performed on grids with different quantities, using the facet average temperature at different height layers as a reference indicator, as shown in Figure 2(c). After conducting the grid independence verification and considering the requirements for computational speed and accuracy, a grid model with 9.85×10^5 grid cells is selected.

2.1.2. Flame images acquisition

The flame images are obtained through the Industrial Flame Monitoring System (IFMS), as shown in Figure 3(a). The monitoring system consists of components such as an air-cooled endoscopic lens tube, camera, motor, recorder, and server. The air-cooled endoscopic lens tube passes through the boiler wall and water-cooled wall at the fire hole above the boiler, capturing the combustion of the flame inside the boiler furnace. The physical appearance of the lens tube is shown in Figure 3(c). The tail end of the air-cooled endoscopic lens tube is connected with the camera, motor, and position switch for controlling the extension and retraction of the lens tube. The physical appearance of the camera, motor, and position switch is depicted in Figure 3(b). The camera converts optical image signals into electrical signals for subsequent transmission. The motor and position switch control the extension and retraction of the lens tube, allowing for adjustment of the shooting position. The image signals are transmitted to the recorder, which converts the electrical image signals into digital signals suitable for storage and transmission. The digital signals are then sent to the server, which is equipped with image processing algorithms. It can perform online image processing calculations when receiving the digital image signals. This allows for the extraction of the required image feature data, which can be displayed and utilized.

Table 1. Main physicochemical phenomena and models of coal combustion (Ye et al. 2022, 2022, 2023).

Physicochemical process	Mathematic model
Gas phase turbulence	Realizable k-ε turbulence model
Particle orbit	Random orbit tracking model
Volatiles pyrolysis	Dual competitive reaction pyrolysis model
Volatile combustion	Unpremixed combustion model
Coke burning	Dynamic/diffusion combustion model
Radiative heat transfer	*p*-1 radiation model
NOx model	Fuel type NOx, thermal type NOx

2.2. Images processing method

2.2.1. Preprocessing

Continuous flame video data is collected through the Industrial Flame Monitoring System (IFMS) installed in the power plant's boiler. Flame images corresponding to different operating conditions are extracted from the video frames, resulting in an initial flame image dataset $F_O(Z_0, Z_1, Z_2, \ldots, Z_n)$. The initial image dataset is then subjected to grayscale conversion and Gaussian denoising filtering, resulting in the image dataset $F_G(Z_0, Z_1, Z_2, \ldots, Z_n)$. Histogram equalization enhancement is performed on the preprocessed images, resulting in the enhanced image dataset $F_H(Z_0, Z_1, Z_2, \ldots, Z_n)$. The Gaussian filtering principle is described by Equation. (1), and the histogram equalization enhancement principle is shown in Equation. (2).

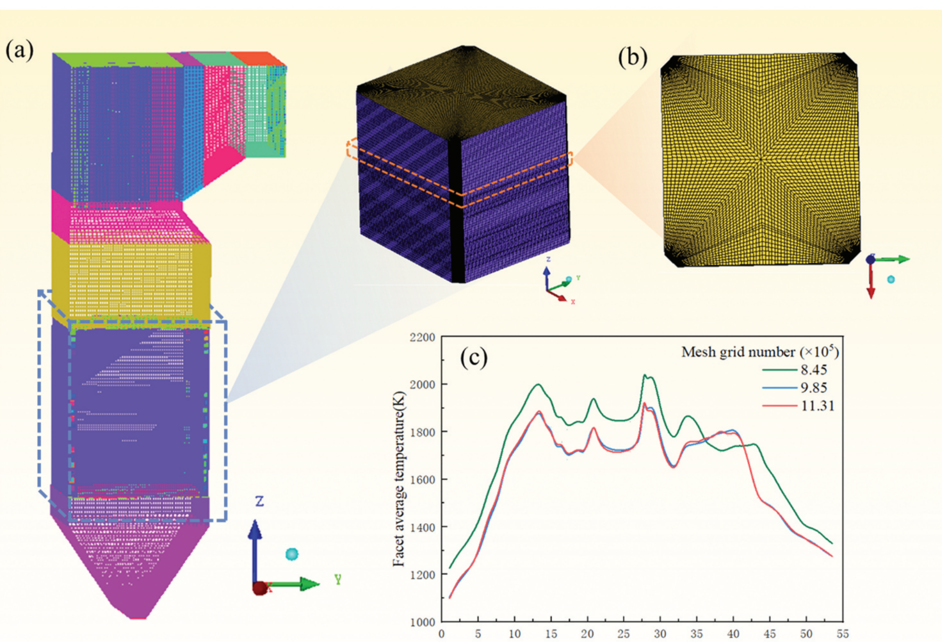

Figure 2. Tangential boiler meshing and independence verification (a)Tangential boiler meshing; (b)Boiler burner area meshing and refinement; (c)Mesh grid independence verification.

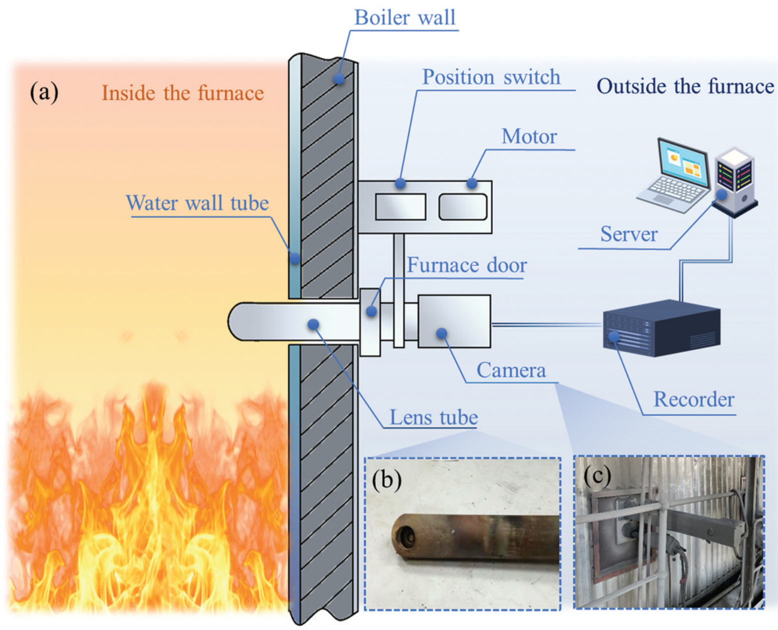

Figure 3. Industrial flame monitoring system (a)System; (b)Camera; (c)Lens tube.

(1) Gaussian filtering (Al-Bulqini et al. 2023; Lingkai and Li 2020)

$$\mathrm{F}(x, y) = \frac{1}{2\pi\sigma^2} e^{-\frac{x^2+y^2}{2\sigma^2}} \tag{1}$$

Among them, x and y represent the pixel coordinates, and σ represents the standard deviation of the Gaussian distribution.

(2) Histogram equalization enhancement (Chaib et al. 2023; Xiong 2020)

$$\mathrm{S_k}(x, y) = \mathrm{T}(r_k) = \sum_{j=0}^{k} P_r(r_j) = \sum_{j=0}^{k} \frac{n_j}{n} \tag{2}$$

Among them, n represents the total number of pixels in the image, n_j represents the number of occurrences of the kth gray level, $P_r(r_j) = \frac{n_j}{n}\left(0 \le r_j \le 1, k = 0, 1, 2, \ldots, L-1\right)$ represents the probability of the kth gray level occurring. Histogram equalization is a process that redistributes the original gray levels based on their probability densities, enhancing the effects of different gray levels in the image and highlighting the image features.

(3) Contour extraction

The preprocessed image dataset F_H is used to create an image sample set. Based on the preprocessed image dataset F_H, the Mask R-CNN algorithm network is constructed to perform segmentation of the high-temperature regions in the tangentially-fired circular flame images.

The structure of the Mask R-CNN algorithm network, as shown in Figure 4, is based on the Faster R-CNN architecture. It replaces the RoI Pooling layer in the original architecture with the RoIAlign layer. The RoIAlign layer uses bilinear interpolation to compute pixel values, avoiding the problem of quantizing the feature regions twice in the original pooling layer. This helps to preserve the floating-point precision, allowing for more accurate coordinate retrieval and feature extraction from the image feature map. Additionally, a Mask

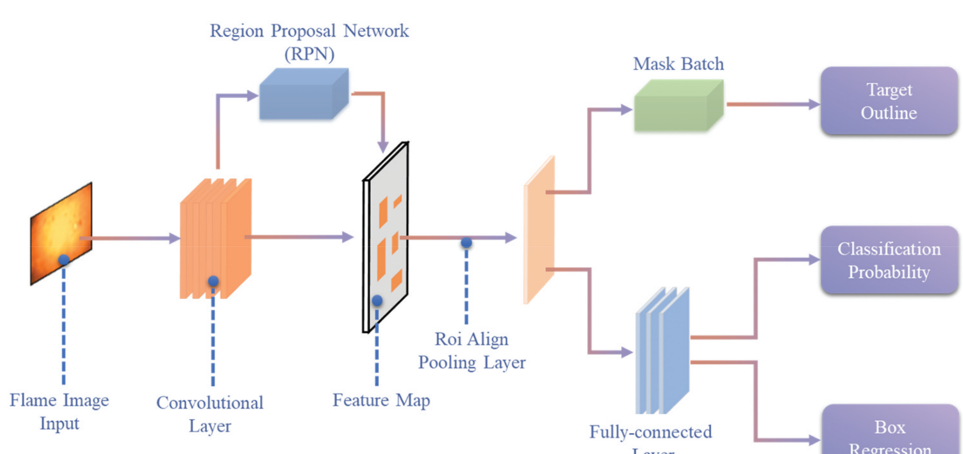

Figure 4. Mask R-CNN model structure (He et al. 2017; Niu, Guo, and Wang 2023; Petrucci et al. 2022).

branch is added in parallel to the network based on the fully convolutional network (FCN) for image region segmentation. This allows for the extraction of the contour of the high-temperature region in the central area of the tangentially-fired circular flame in the two-dimensional flame images.

The flame image dataset is fed into the ResNeXt convolutional network, which generates five different scale convolutional feature maps, namely P2 to P6. The FPN (Feature Pyramid Network) is then applied to the convolutional feature maps, performing 2× upsampling and fusion to obtain the multi-scale feature maps, referred to as Tmaps. Additionally, several region of interest (ROI) proposals are generated on the convolutional feature maps. The ROIAlign pooling operation is performed on the Tmaps, which involves quantizing the image pixels during the mapping process and utilizing bilinear interpolation for scaling. This process results in fixed-sized floating-point feature maps, denoted as TROI. The TROI is passed through fully connected layers, which provide predictions for class labels, rectangular regions, and segmentation areas. This completes the training process of the model.

The model evaluation metrics include precision and recall. Precision (P) measures the proportion of successfully predicted segmented flame core high-temperature area images to the total number of predicted segmented contours. Recall (R) measures the proportion of successfully predicted segmented flame core high-temperature area images to the total number of flame core high-temperature area images in the sample.

In addition, considering the characteristics of the tangentially-fired circular boiler combustion flame, the average contour area ratio is included as a quality evaluation for the extraction of the circular flame core high-temperature area. It represents the average ratio of the predicted segmented contour area to the actual high-temperature area of the flame core.

The Precision (P) and Recall (R) are shown as Eq. (3)-(4).

$$P = T_P/(T_P + F_P) \tag{3}$$

$$R = T_P/(T_P + F_N) \tag{4}$$

In the equations provided, T_P represents the number of flame core high-temperature areas that have been correctly segmented in the model's predictions. F_P represents the number of non-flame core high-temperature areas that have been erroneously segmented in the model's predictions. F_N represents the number of flame core high-temperature areas that have not been segmented in the model's predictions.

The average contour area ratio is shown in Equation. (5).

$$\alpha_C = \frac{\sum_1^n H}{n}/C \tag{5}$$

H represents the covered area of the contours calculated by the model's predictions. C represents the covered area of the contours labeled in the annotated flame images and n represents the number of samples in the experiment.

2.2.2. Feature extraction

Using Mask R-CNN, the enhanced flame images $F_H(Z_0, Z_1, Z_2, \ldots, Z_n)$ are segmented to obtain the core combustion regions. This process results in the effective flame image regions $F_{R-CNN}(Z_0, Z_1, Z_2, \ldots, Z_n)$ corresponding to each frame of the operating conditions. Additionally, the corresponding effective contours $L_{R-CNN}(Z_0, Z_1, Z_2, \ldots, Z_n)$are obtained for these regions.

The effective flame image regions, $F_{R-CNN}(Z_0, Z_1, Z_2, \ldots, Z_n)$, is processed using a multi-level feature extraction model. Firstly, the area H of the flame core region contour is calculated, as shown in Equation. (6). Within this region, the flame's center coordinates W_x and W_y are computed based on the area, as shown in Equation. (7) and (8).

(1) Flame region area

$$H = \oint_L F(x,y) \cdot dr = \iint_L Pdx + Qdy \tag{6}$$

where $F(x,y)$ is the feature contour vector function, and P and Q are two components of the $F(x,y)$.

(2) Flame center

$$W_x = \frac{\iint^x F(x,y)dH}{H} \tag{7}$$

$$W_y = \frac{\iint^y F(x,y)dH}{H} \tag{8}$$

where W_x represents the center x coordinate, and W_y represents the center y coordinate.

Additionally, to ensure the reliability of the modification, an analysis of the fluctuations in the flame center is performed. The flame center deviation between frames is calculated, as shown in Equation. (9) to remove frames with excessive fluctuations.

$$\text{O\_deviation} = \frac{\sum_{n=i} \sqrt{(x_i - x_1)^2 + (y_i - y_1)^2}}{n} \tag{9}$$

where x_1 and y_1 are the center coordinates in the first frame, x_i and y_i are the center coordinates in the i-th frame, and n is the number of frames selected for sampling.

The flame image information undergoes abnormal frame cleaning using a dynamic window and flame center deviation for anomaly detection. In this paper, the image acquisition device can capture images at a rate of 30 frames per second (FPS). Therefore, A continuous window with a width of 30 frames per second (FPS) is utilized, as shown in Equation. (10).

$$\{z_0, z_1, z_2 \ldots\ldots z_i, z_{i+1} \ldots z_j \ldots\ldots z_n\}$$

$$i \in [0, n-k]; j \in [i+k-1, n-1] \tag{10}$$

where i is the starting position of the dynamic window, j represents the ending position of the dynamic window, and k represents the width of the dynamic window. In this paper, a window width of 30 is used.

The flame images captured between frames are preprocessed, and the flame center deviation is calculated. This deviation is compared to a threshold δ. If it surpasses the abnormal threshold δ, the frame is identified as a cleaning object. The δ calculation is based on a 1K change in the temperature of the heat transfer tube inside wall. The corresponding fluctuation in the flue gas temperature is ± 5 to ± 7K. In the actual boiler operation, during each second operating interval, the temperature fluctuations of the flue gas near the pipe wall do not exceed the aforementioned values. This fluctuation, as observed in the numerical temperature field, corresponds to a center deviation of approximately ± 0.3 to ±0.4 m. When considering the boiler dimensions, this deviation is equivalent to approximately ± 2.5% of the overall size.

2.3. Temperature modified method

Based on the geometric and intensity features extracted from flame images processing, the temperature field obtained from numerical simulations is modified for temperature distribution using the temperature field modification scheme, as shown in Figure 5(a).

Firstly, matching numerical temperature field distributions and flame feature modification matrix are obtained separately through numerical simulation methods and flame image feature extraction. The nearest neighbor algorithm is used to map and match grid points, forming a structured grid model. Figure 5(b) shows a cross-sectional view of the boiler's regularized grid along the height direction.

Flame images are collected under the same operating conditions as the numerical temperature field, and combustion feature extraction is performed on these flame images to obtain relevant features of flame combustion. Then, an abnormality evaluation is performed on the flame center deviation between each frame, and if the flame center deviation fluctuates less than δ between frames, the next step of matrix modification for the numerical temperature field is carried out.

The center features of the flame images are used to compute the center feature modification matrix in the corresponding structured grid model. The calculation method for each grid is shown in Equation. (11), resulting in the formation of the modification matrix. The procedure of the matrix formed is shown in Figure 5(c).

$$F(i,j) = \sum_{m}\sum_{n} x(i+m, j+n)w(m,n) \tag{11}$$

where $F(i,j)$ represents the feature ratio at the corresponding position of the feature matrix, $x(i,j)$ represents the feature value of the flame image pixel, and $w(m,n)$ represents the proportional kernel function, m, n indicate the proportional size of the kernel function.

The center feature modification matrix is used to modify the numerical temperature field. The coefficient at each corresponding position in the grid is multiplied with the temperature field parameters of the numerical temperature field through matrix operations, as shown in Equation. (12), resulting in the temperature parameters affected by the center

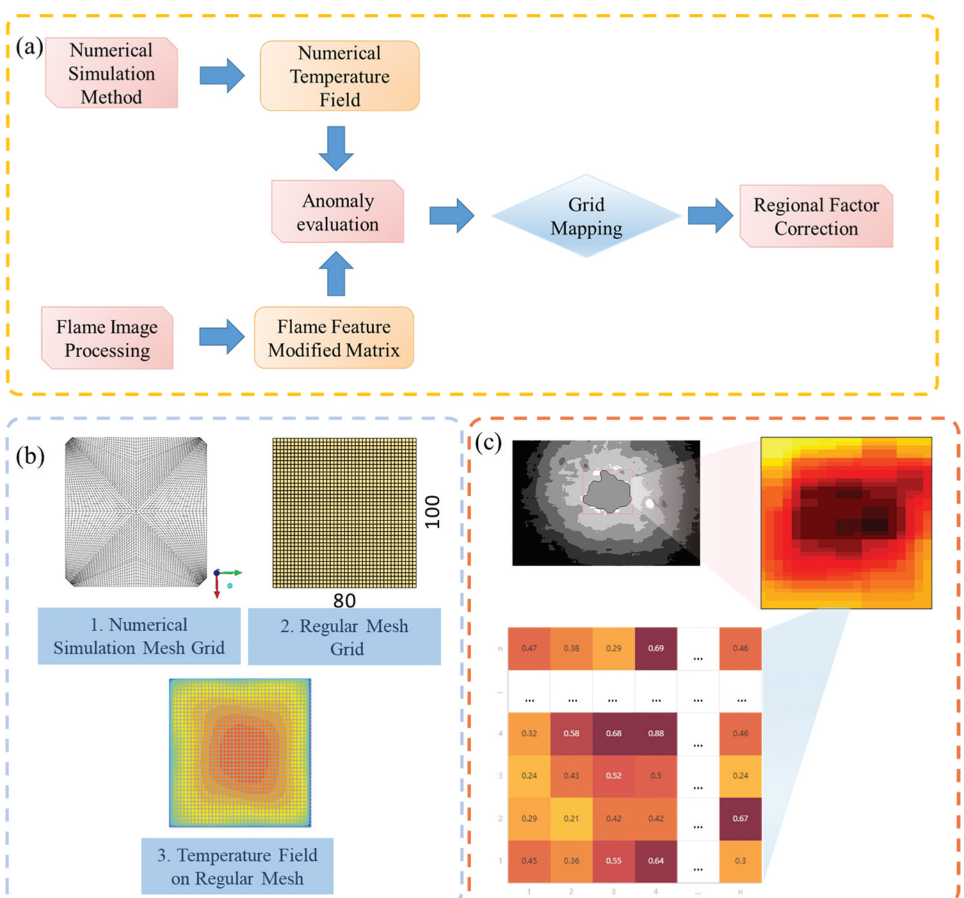

Figure 5. Temperature modified method: (a) Temperature field matrix modification scheme; (b) Mesh grid regularization; (c) Central modification matrix.

modification matrix. After processing all the matching grids, the numerical temperature field distribution influenced by the combustion center offset is obtained.

$$M(i,j) = \sum_{m}(F(i,k) \times S(k,j)) \quad (12)$$

where $M(i,j)$ represents the modified numerical temperature field, $S(k,j)$ is the original numerical simulation temperature field on regular mesh.

3. Results and discussions

3.1. CFD result analysis

Six different load conditions are selected as validation scenarios for numerical simulation results based on the historical operating parameters from the DCS system of the power plant boiler. The historical operating parameters for these six operating conditions are shown in Table 2. Additionally, the coal characteristics corresponding to these six historical boiler operating conditions are shown in Table 3.

Based on the operational parameters obtained from the DCS, the physical and chemical model specified in Table 1 is used for simulation. The simulation employs the Semi-Implicit Method for Pressure Linked Equations (SIMPLE) computational method. The pressure term is calculated using a second-order format, while the diffusion and convection terms are computed using a second-order upwind format. The simulation continues until the residual of each equation is less than 1×10^{-3}, indicating convergence of the calculations. The numerical simulation of the boiler involves the process of heat and mass exchange. Therefore, after the simulation calculations converge, the results are validated from both the energy and mass perspectives to ensure their reliability.

The validation of the simulation results is carried out from an energy perspective, as shown in Figure 6(a) and (b). The energy parameters at the inlet and outlet of the boiler for the six typical operating conditions are compared to verify the energy conservation within the computational domain, as illustrated in Figure 6(a). From the graph, it can be observed that the energy levels increase steadily with increasing load for different operating conditions, and the energy conservation at the inlet and outlet of the simulation domain has a relative error below 2%. In addition to overall energy conservation, it is necessary to compare the simulated result parameters with the measured parameters at the actual boiler operating points. Figure 6(b) shows the comparison between the simulated and calculated values of the heat exchange in the furnace for different operating conditions. It can be observed that the heat exchange in the water-cooled wall of the furnace has the highest proportion, while the heat exchange in the partition panel and rear plate superheater is comparable. The simulated heat absorption by these three heating surfaces is in agreement with the calculated heat exchange based on the boiler temperature measurements.

From a mass exchange perspective, the convergence of the CFD results is validated, as shown in Figure 6(c) and (d). The inlet and outlet mass parameters of the CFD results for different operating conditions are compared to verify the conservation at the boundaries of the computational domain, as illustrated in Figure 6(c). From the graph, it can be observed that the mass is perfectly conserved at the inlet and outlet of the computational domain. Due to the very small relative errors, absolute errors in mass are calculated. The absolute errors for the inlet and outlet of different operating conditions remain below 0.01, thus the errors can be considered negligible. Figure 6(d) presents a comparison between the simulated and measured values of O_2 and NO emissions at the furnace

Table 2. Operating condition of boiler numerical simulation.

Boiler operating condition	Load 1	Load 2	Load 3	Load 4	Load 5	Load 6
Boiler load(%)	69.80	71.98	74.55	77.06	79.86	84.07
Coal feed rate of coal feeder A (kg/s)	27.87	32.17	29.93	30.58	32.32	29.30
Coal feed rate of coal feeder B (kg/s)	27.83	29.66	29.94	31.19	33.54	35.44
Coal feed rate of coal feeder C (kg/s)	26.18	33.02	25.01	31.11	35.15	36.59
Coal feed rate of coal feeder D (kg/s)	27.18	29.55	30.04	30.59	32.04	33.56
Coal feed rate of coal feeder E (kg/s)	−0.05	1.24	−0.05	0.06	0.09	−0.06
Total primary air volume (Nm^3/h)	258.63	272.61	282.16	296.45	305.75	313.17
Total secondary air volume (Nm^3/h)	458.76	442.60	488.64	522.30	556.36	580.51
A Inlet air volume (Nm^3/h)	48.39	52.29	56.87	58.91	59.51	57.14
B Inlet air volume (Nm^3/h)	51.25	52.05	56.02	58.55	54.51	56.34
C Inlet air volume (Nm^3/h)	55.52	53.36	53.69	56.28	52.15	56.63
D Inlet air volume (Nm^3/h)	50.45	52.62	51.72	52.65	50.16	51.58
E Inlet air volume (Nm^3/h)	0.05	0.06	0.08	0.06	0.08	0.03

Table 3. Properties of coal of typical operating condition.

	Proximate analysis(%,ar)					Ultimate analysis(%,ar)				
Condition	Mar	Aar	Var	Fc,ar	Qar,net (MJ/kg)	Car	Har	Oar	Nar	Sar
Load 1	17.12	13.35	25.27	44.26	19.66	49.98	4.43	13.53	1.03	0.56
Load 2	16.56	14.99	25.09	43.36	20.75	55.90	2.95	8.03	1.02	0.56
Load 3	16.18	19.26	23.45	41.11	19.51	50.25	3.74	9.24	0.96	0.37
Load 4	19.58	12.52	25.39	42.51	20.05	54.52	2.92	9.07	1.02	0.37
Load 5	16.66	14.30	25.66	43.38	20.33	54.91	3.02	9.52	1.03	0.56
Load 6	15.68	17.59	24.18	42.55	19.14	51.43	3.00	10.18	0.99	1.14

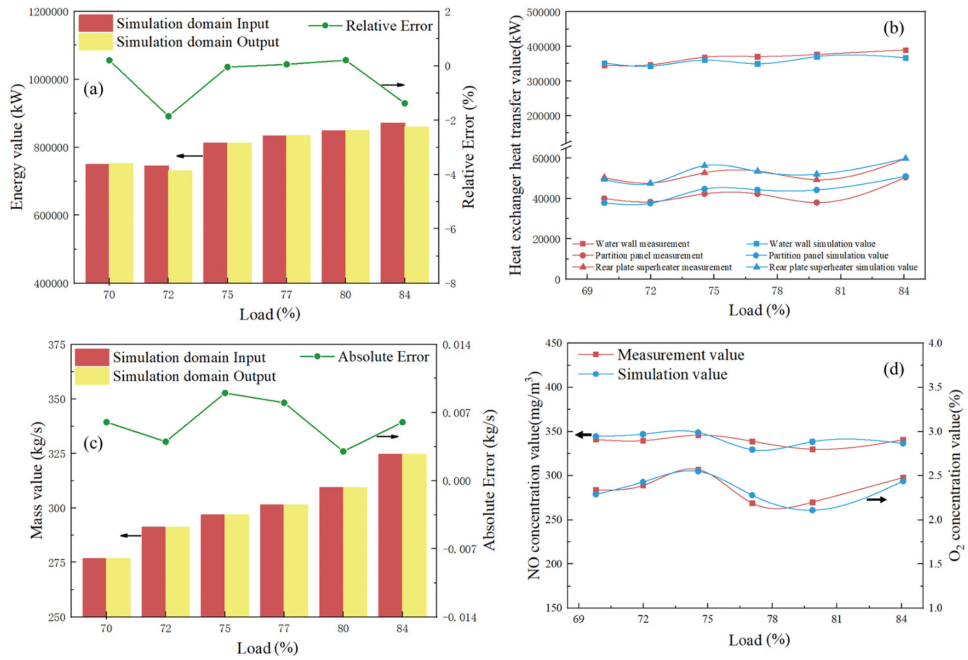

Figure 6. Energy and mass analysis: (a)Energy conservation; (b)Heat exchanger heat balance analysis; (c)Mass conservation; (d) Furnace outlet flue gas O2 and NO value analysis.

flue gas outlet. The DCS provides real-time monitoring of the O_2 and NO concentrations at the furnace outlet. By converting the measured O_2 content and the mass flow rate of NO at the outlet for different operating conditions, a comparison is made with the numerical values of O_2 and NO obtained from the CFD results. The graph shows that the numerical values of O_2 and NO at the outlet for different operating conditions align with the actual measurement results.

In addition to the overall mass conservation, the conservation of key combustion components in the inlet and outlet is also compared and validated, as shown in Table 4. The table illustrates the conservation of carbon, hydrogen, oxygen, and nitrogen, which are the four main components. The relative errors for these components at the inlet and outlet are under 3.05%, indicating the conservation of mass and composition for different operating conditions.

Figure 7 shows the temperature field distribution in different regions of the boiler, using Load 6 as an example. In the burner region, the height temperature field distribution at injections A, B, C, and D exhibits a centrally symmetrical pattern. The inflow at the four corners is distinct, creating a swirling combustion in the center. As the height increases, the central circular section gradually narrows, forming a high-temperature area that connects in the D-layer section. Moving up to the SOFA region, the injections of SOFA air ensure thorough coal powder combustion. In the transitional region, the swirl weakens, and the distribution of high-temperature areas transitions from a cruciform shape to an approximate rectangular shape. In the flame corner region, an elliptical high-temperature area gradually takes shape.

It also can be observed that the temperature field exhibits a centrally symmetrical distribution, and the inflow at the four

Table 4. Component fraction conservation analysis.

		Elements (kg/s)			
Load (%)	Items	C	H	O	N
69.80	Simulation domain Input	18.90	1.57	67.51	208.80
	Simulation domain Output	18.49	1.56	68.37	202.49
	Relative Error (%)	−2.169	−0.637	1.274	−3.022
71.98	Simulation domain Input	18.65	1.7000	71.47	219.69
	Simulation domain Output	18.37	1.7002	72.81	213.01
	Relative Error (%)	−1.501	0.012	1.875	−3.041
74.55	Simulation domain Input	20.46	1.73	71.67	219.58
	Simulation domain Output	19.95	1.72	73.14	213.09
	Relative Error (%)	−2.493	−0.578	2.051	−2.956
77.06	Simulation domain Input	20.86	1.81	73.42	225.76
	Simulation domain Output	20.43	1.83	72.01	220.54
	Relative Error (%)	−2.061	1.105	−1.920	−2.312
79.86	Simulation domain Input	21.35	1.85	74.98	233.45
	Simulation domain Output	21.09	1.84	75.66	230.99
	Relative Error (%)	−1.218	−0.541	0.907	−1.054
84.07	Simulation domain Input	21.66	1.900	78.19	239.47
	Simulation domain Output	21.35	1.901	79.63	232.23
	Relative Error (%)	−1.431	0.051	1.842	−3.023

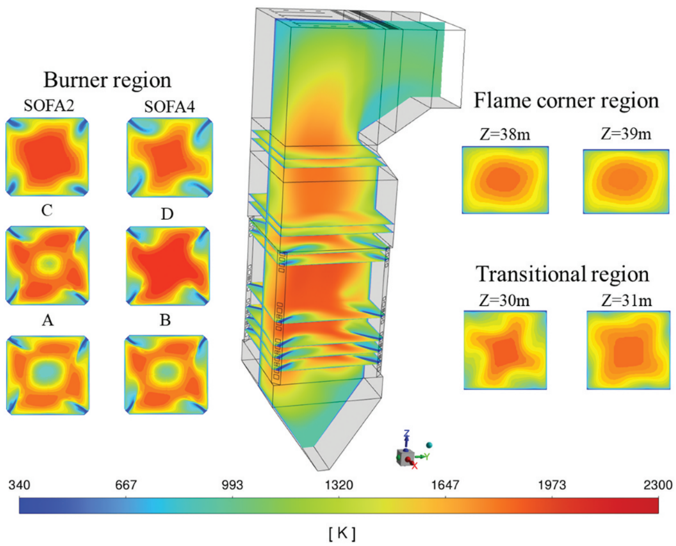

Figure 7. Numerical temperature field.

corners is relatively uniform. As the height increases, the high-temperature center of the flame is located at the geometric center of the furnace. However, in actual boiler operation, the flame center often deviates from the geometric center of the furnace. Due to long-term operation, factors such as ash accumulation and wear can lead to changes in the resistance of the air duct, resulting in differences in the stiffness of the inflow at the four corners. This leads to an uneven inflow, causing the flame center to shift. During boiler operation, the displacement of the flame center can result in uneven heating of the water-cooled walls surrounding the boiler. This can cause overheating on one side of the water-cooled wall heat exchangers, leading to a large number of tube failures and severely impacting the long-term safety of equipment operation.

When conducting numerical simulations for square corner tangential firing, it is commonly assumed that the parameters of the corner nozzles are uniformly distributed for the simulation calculations. This assumption of uniformity in the corner firing can result in symmetric temperature field distribution in the simulation results. To ensure accurate representation of the numerical temperature field in both macroscopic conservation and distribution details, it is essential to incorporate on-site boiler monitoring information for online modification. Flame images can capture the combustion situation inside the furnace. Therefore, by extracting features from flame images, it is possible to modify the numerical temperature field.

3.2. Flame images analysis

3.2.1. Flame images enhancement

By segmenting the flame videos, flame images for each frame are obtained. The image size is standardized to 960px × 720px, forming a dataset of flame images. An example of the original flame image dataset is shown in Figure 8(a). For ease of representation, the original flame images data is labeled as $F_O(Z_0, Z_1, Z_2, \ldots, Z_n)$. As shown in Figure 8(a), these are the flame images corresponding to Load 1-Load 6 in Table 2. As the load increases, the brightness of the flame intensifies, and the central white area becomes more prominent.

The original flame images data is preprocessed by converting them to grayscale and applying Gaussian noise filtering. This preprocessing step produces a new set of images, denoted as $F_G(Z_0, Z_1, Z_2, \ldots, Z_n)$, as shown in Figure 8(b).

Building upon the Gaussian noise reduction, further enhancement is applied to the flame images. After performing histogram equalization, the preprocessed image set $F_H(Z_0, Z_1, Z_2, \ldots, Z_n)$ is obtained, as shown in Figure 8(c). The contrast of the flame images is improved, making the distinction between the flame center and the surrounding edges more pronounced. The high-temperature region at the flame center appears as bright white, highlighting the contrast between the flame center and the edges. This enhancement is advantageous for flame images segmentation and feature extraction tasks, as it makes the flame regions more distinct and identifiable.

3.2.2. Flame core area contour extraction

The Mask R-CNN model from section 2.2.1 is used to extract the contours of the flame's core area. The model is trained and validated, and the evaluation results on the test dataset are presented in Table 5. As shown in Table 5, the Mask R-CNN model achieves a precision of 92.35% and a recall of 90.44% in extracting the high-temperature regions of the flame accurately. Regarding the predicted segmented contours, the average contour area accounts for 95.85% of the total area. This essentially covers the core high-temperature region of the circular combustion flame in the four-corner tangentially fired coal boiler. These results demonstrate that the model achieves precise and efficient segmentation during its offline training process.

The converged model is applied to extract the contours of the high-temperature regions for the validation operating conditions of Load 1-Load 6. The resulting dataset of flame image contour extraction is denoted as $F_{R-CNN}(Z_0, Z_1, Z_2, \ldots, Z_n)$, as shown in Figure 9. The extracted core contours are highlighted using masks and bounding rectangles. Throughout the load variation process, from low to high, the extraction of the core high-temperature region of the circular combustion flame in the four-corner tangentially fired boiler remains stable. The extraction of the flame's core high-temperature region edges is relatively accurate. As the load increases, the core high-temperature region of the flame gradually expands. During the processing of turbulent fluctuating flame variations, there is minimal interference from contour features of other regions. This method effectively adapts to the features of flame edge fluctuations and preserves the overall geometric distribution of the flame. It provides a basis for subsequent calculations related to the overall flame, geometric features of the flame's core region, and its distribution characteristics, allowing for further analysis of flame features based on image samples.

3.3. Flame images feature extraction

Based on the feature extraction method described in section 2.2.2, feature parameters can be calculated. As shown in Figure 10(a), we define the furnace center and the corresponding coordinate system, where the boiler center is designated as

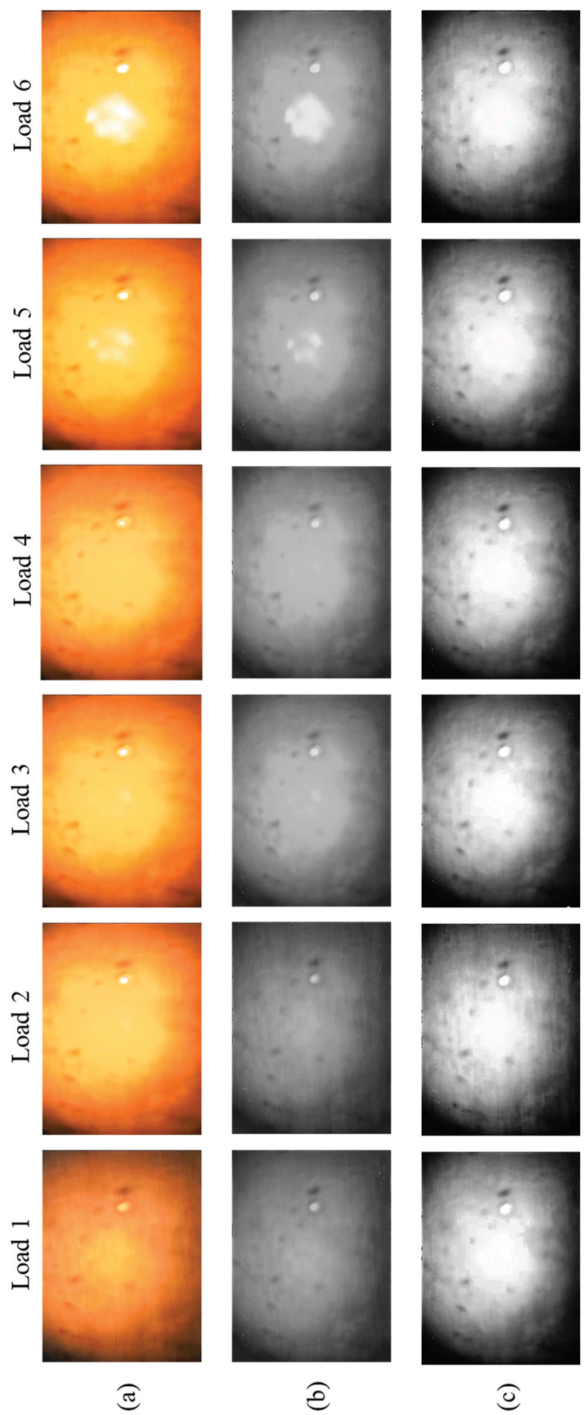

Figure 8. Flame images enhancement: (a)Original flame images data; (b)Gaussian filtering; (c)Image enhancement.

Table 5. Mask R-CNN effect evaluation of region contour extraction.

Evaluation index	Value
TP	7678
FP	636
TN	674
FN	812
P	92.35%
R	90.44%
α_C	95.85%

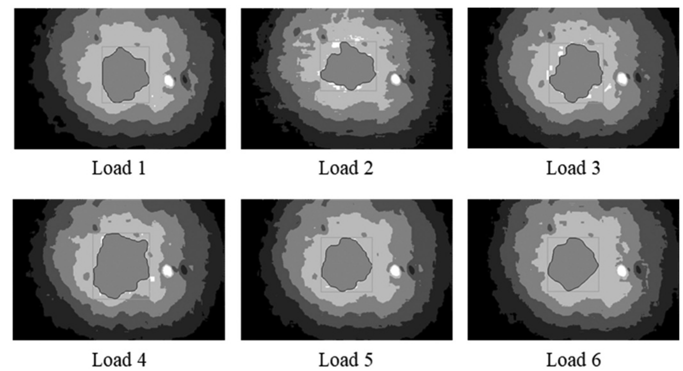

Figure 9. Mask R-CNN area segmentation effect.

the origin point (O). The y-direction points from the front wall to the back wall of the boiler, and the x-direction points from the right side wall to the left side wall of the boiler. As depicted in Figure 10(b), the coordinates of the circular combustion flame center are obtained from the preprocessed flame images dataset $F_{R-CNN}(Z_0, Z_1, Z_2, \ldots, Z_n)$. It is evident that the flame centers obtained under different operating conditions exhibit noticeable offsets and fluctuations.

By calculating the deviation between the flame center and the boiler center coordinates, as shown in Figure 10(c), it is evident that the y-coordinate deviation of the flame center in this load condition is relatively small, fluctuating around the y = 0 position. This type of fluctuation is caused by the turbulence and pulsation in the combustion process, indicating reasonable deviations in the y-direction. However, significant deviations are observed in the x-coordinate direction of the flame center. Specifically, in the current operating condition, the flame centers consistently exhibit a shift toward the negative x-direction, toward the right side wall of the boiler. The maximum deviation distance reaches up to 1.3 meters. If such one-side deviations persist over the long term, it will result in uneven heating around the boiler, leading to prolonged overheating of the water-cooled wall on one side. This can ultimately cause extensive damage and ruptures in the heat exchange tubes of the water-cooled wall on that side, posing a risk to the safe operation of the boiler.

3.4. Temperature field modification

This experiment considered the feasibility of on-site application by setting up a computational server at the coal-fired boiler site for numerical temperature field modification processing. The computational server is connected to the coal-fired boiler's DCS

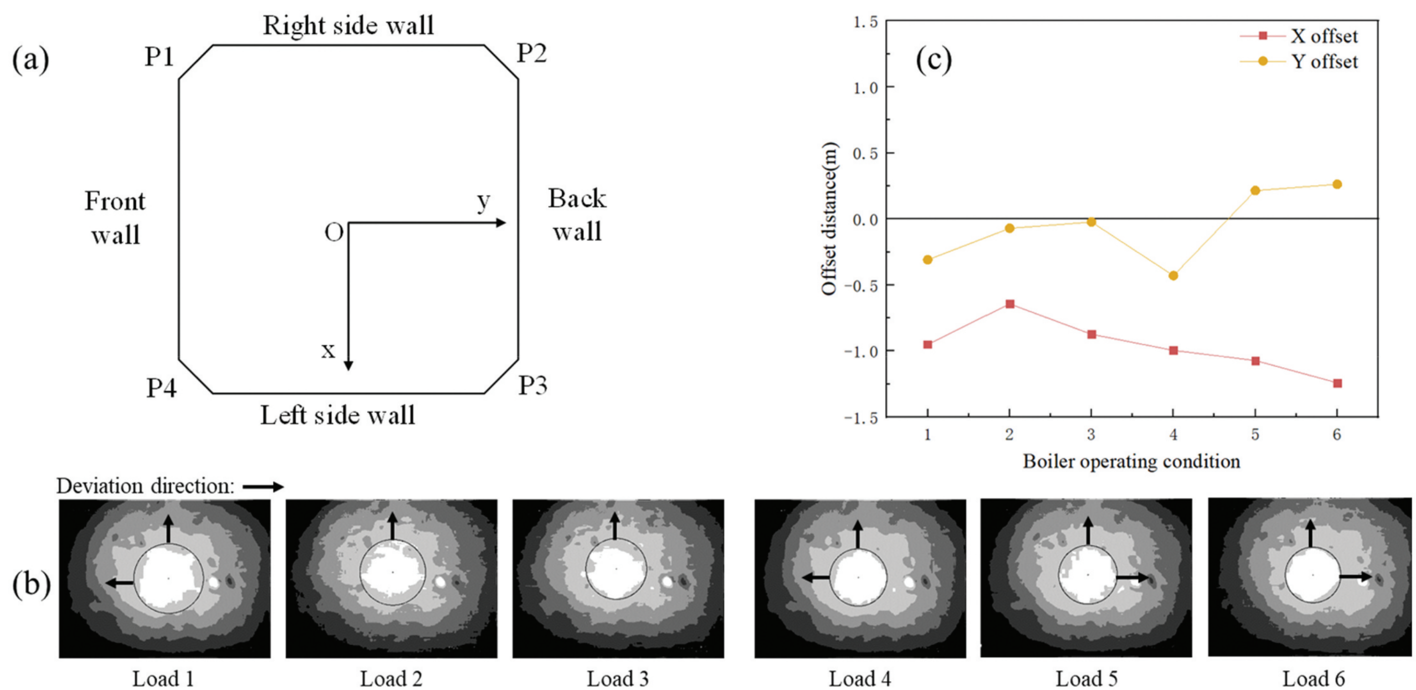

Figure 10. Flame images center feature: (a)Boiler x, y orientation map; (b)Flame center position; (c)Flame center deviation distance.

and IFMS through the Webservice and TCP port. The computational resources of the server utilize an Intel XEON E5-2630V4 CPU and NVIDIA GeForce RTX 2080 Ti GPU. The research on numerical temperature field modification is conducted on the aforementioned computational platform.

Using the modification method described in section 2.3, the center modification matrix related to the geometric features of the flame images are calculated. The numerical temperature field is then modified through matrix operations to obtain the modified temperature field distribution. Taking the boiler operating condition of Load 6 as an example, the furnace area is analyzed by selecting cross-sections at each nozzle height. The temperature field modification results are shown in Figure 11. Figure 11(a) displays the distribution of the numerical temperature field before modification. It can be observed that the temperature field distribution at different height levels exhibits symmetry, with the combustion center located at the geometric center of the boiler. Particularly in the area of the SOFA region, the highest temperature region of combustion is primarily located at the center, and the inflow intensity of the four corner jets is relatively consistent. Moreover, the modified numerical simulation results indicate that the flame does not significantly adhere to the burner wall.

Figure 11(b) illustrates the temperature field distribution after flame feature modification. It is evident that the circular center of the flame in the corner jets has shifted toward the upper right direction, causing a noticeable upward displacement of the high-temperature region of the combustion flame. This leads to significant wall adherence near the right-side wall and back wall of the boiler. Consequently, overheating of the water-cooled wall tubes in the wall adherence areas can occur, resulting in tube failure due to overheating.

Above the burner region is the transitional region and the flame corner region. The temperature distribution modification changes near the height interfaces of the transitional zone and corners are observed, as shown in Figure 12. In Figure 12(a), it can be observed that in the transitional zone, the modified temperature field distribution exhibits a diagonal cross-like pattern, gradually transforming into a nearly square shape as the height increases. As the height increases to the flame corner region, the temperature field distribution forms an elliptical shape with a central distribution. After modifying the numerical temperature field, in Figure 12(b), it is evident that in the transitional zone, the temperature distribution shifts noticeably toward the upper right corner, forming a triangular pattern. The temperature distribution gradually changes into an elliptical shape in the flame corner region as the height increases. However, after modification, the temperature field's combustion center also shifts toward the upper right corner, exhibiting a proximity to the right-side wall and back wall of the furnace.

Through qualitative analysis, it can be observed that the trend of temperature field modification is consistent with the image trend, showing a shift toward the right-side wall and back wall of the boiler furnace. The modified temperature field is closer to the actual situation compared to the numerical temperature field obtained from CFD under the assumption of uniform distribution in the corners.

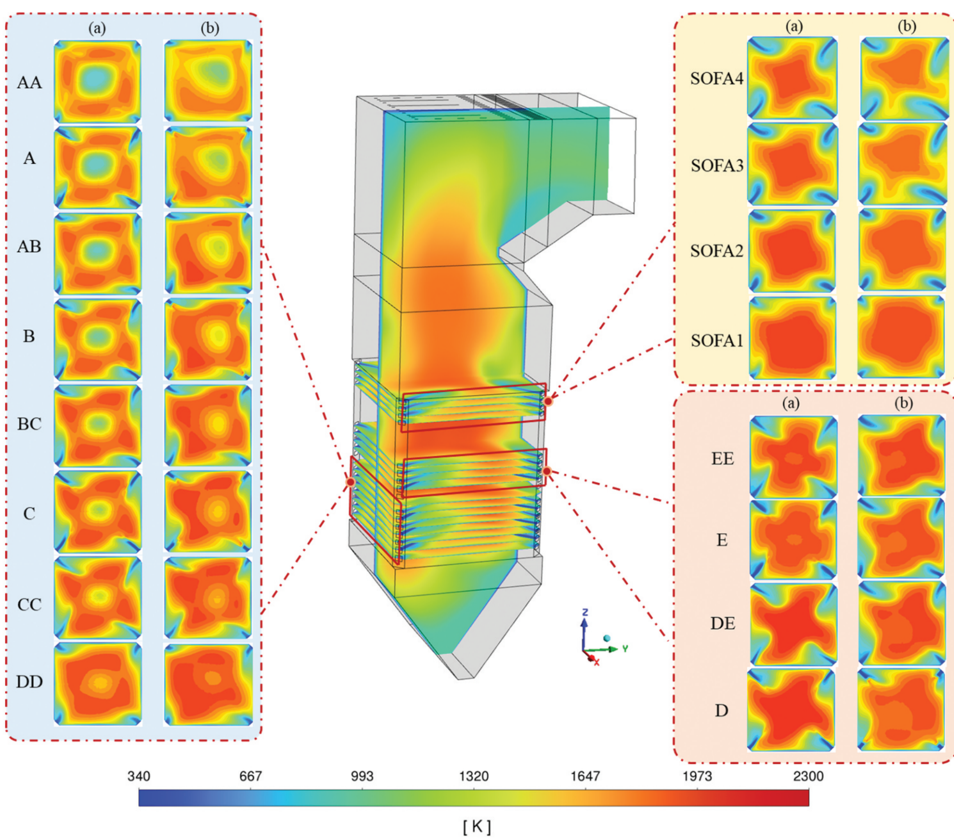

Figure 11. Flame center modified numerical temperature field:(a)Before modified, (b)After modified.

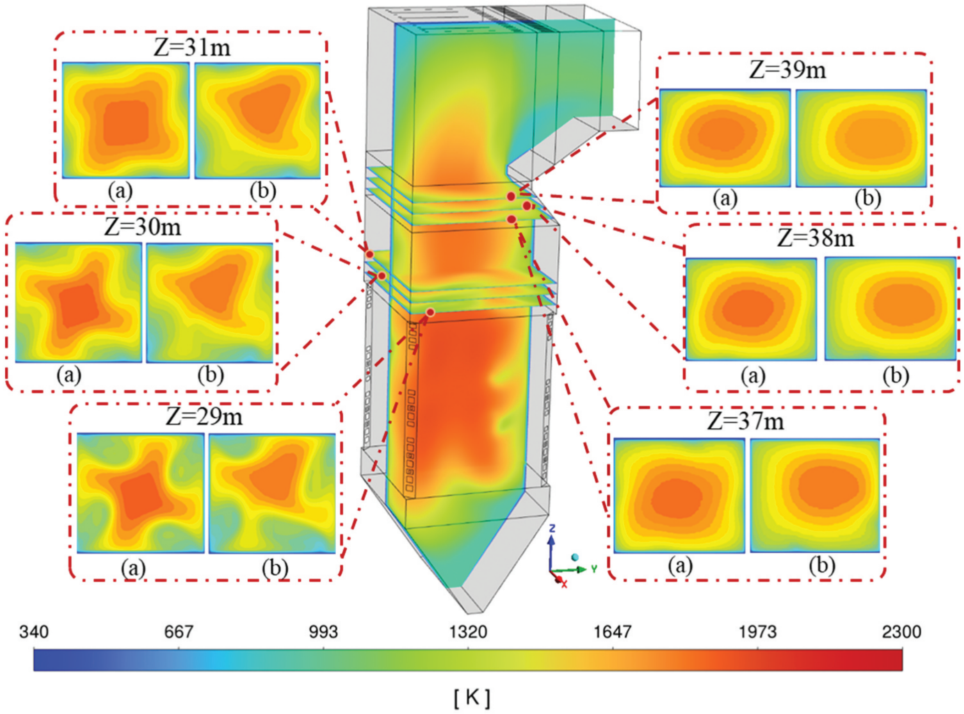

Figure 12. The temperature field distribution in different height cross-sections of the transitional zone: (a)Before modified, (b)After modified.

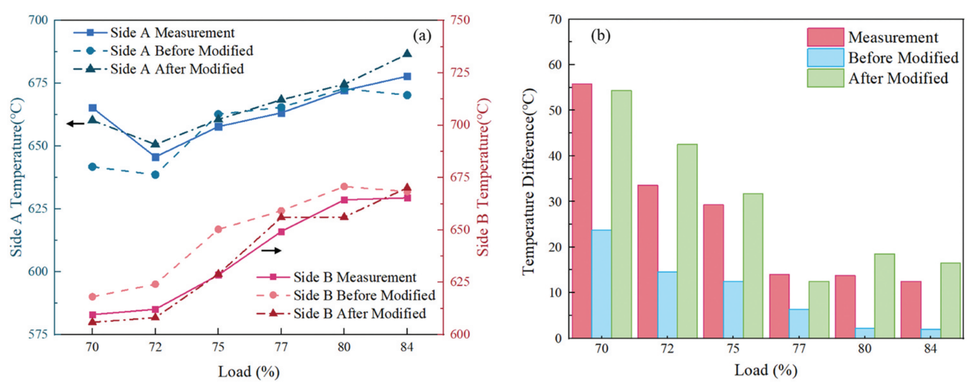

Figure 13. Modified temperature field verification: (a)Side a and B temperature value comparison; (b)Temperature difference between side a and B.

In a tangential boiler, the cut corners create swirling airflow, resulting in residual rotation at the furnace horizontal flue. This residual rotation leads to temperature deviations in the flue gas above the flame corner region. When the combustion center is offset, the temperature deviations caused by residual rotation become more pronounced. The measurement of residual rotation is performed by placing two measurement points, referred to as the side A and side B measurement points, as shown in Figure 1(b), at the right wall and left wall of the boiler flue.

Figure 13(a) presents a line graph comparing the temperature fields before and after modification with the actual measurement data at sides A and B. The graph shows that on the side A, the temperature trend of the modified temperature field aligns with the actual measurement values and is slightly higher than the values before modification. On the B side, the modified temperature values are noticeably lower than before modification, aligning better with the actual measurement values. The absolute error between the modified temperature field and the measurement values is below 8.8K, with a relative error below 1.3%. Additionally, the temperature difference between the A and B sides, as shown in Figure 13(b), provides a clearer indication of temperature deviations. Compared to the results before modification, the temperature differences between the two sides become more pronounced after modification and are closer to the temperature differences of actual measurement. In summary, the temperature distribution after modification, based on flame image features, reflects the deviation of the flame center and aligns more closely with the actual boiler operation.

4. Conclusions

In this study, a method is proposed to modify the CFD numerical simulation temperature field using the flame image features of the boiler furnace. The application of this method enables the CFD numerical simulation temperature field to be more consistent with the actual operating conditions inside the boiler furnace. The following conclusions are drawn:

(1) The CFD numerical simulation is conducted on a tangentially-fired boiler, and simulation results are obtained for different operating conditions with convergence. The simulation results are validated based on energy and mass conservation. Further analysis of the numerical temperature field's detailed structure shows a centrally symmetrical distribution. However, it is found that the assumption of uniform inflow at the four corners did not accurately reflect the actual displacement of the flame center in the operational boiler.
(2) The boiler flame is captured through a flame monitoring system. Preprocessing operations such as noise reduction filtering, enhancement, and contour extraction are applied to extract the combustion characteristics of the boiler flame. The flame center feature exhibits a noticeable shift toward the right-side wall of the boiler, with a displacement distance of up to 1.3 m. This results in uneven heating of the surrounding water-cooled walls.
(3) The modified temperature field, based on flame features, shows a center deviation toward the right-side wall and back wall of the furnace. By comparing with actual flue gas temperature measurements, it is found that the modified temperature trend aligns more closely with the actual data, with an absolute error below 8.8 K and a relative error below 1.3%. Compared to the results before modified, the modified temperature field better reflects the actual operating conditions of the boiler.

Acknowledgements

The research was supported by the National Natural Science Foundation of China (No. 52376107), and Guangdong Basic and Applied Basic Research Foundation (2022A1515010709). We also acknowledge the support from the Fundamental Research Funds for the Central Universities (2022ZFJH04) and Guangdong Province Key Laboratory of Efficient and Clean Energy Utilization (2013A061401005).

Disclosure statement

We declare that we have no known competing financial interests or personal relationships that could have appeared to influence the work reported in this paper.

Funding

The work was supported by the Basic and Applied Basic Research Foundation of Guangdong Province [2022A1515010709]; Fundamental Research Funds for the Central Universities [2022ZFJH04]; Guangdong Key Laboratory of Efficient and Clean Energy Utilization, South China University of Technology [2013A061401005]; National Natural Science Foundation of China [No. 52376107].

ORCID

Youcai Liang http://orcid.org/0000-0002-0671-2952

Nomenclature

Abbreviations	
CFD	Computational Fluid Dynamics
Mask R-CNN	Mask Region-based Convolutional Neural Network
A	A layer of primary air
B	B layer of primary air
C	C layer of primary air
DD	DD layer of auxiliary air
DE	DE oil auxiliary air
EE	EE layer of auxiliary air
SOFA2	Separate over fire air 2
SOFA4	Separate over fire air 4
RE	Relative error
Symbol	
M_{ar}	Moisture as received coal
V_{ar}	Volatiles as received coal
$Q_{ar,net}$	Lower heating value as received coal
H_{ar}	Hydrogen content as received coal
N_{ar}	Nitrogen content as received coal
F_O	Initial flame image dataset
F_H	Histogram equalization enhancement image dataset
DCS	Distributed Control System
AA	AA layer of auxiliary air
AB	AB oil auxiliary air
BC	BC oil auxiliary air
CC	CC layer of auxiliary air
D	D layer of primary air
E	E layer of primary air
SOFA1	Separate over fire air 1
SOFA3	Separate over fire air 3
AE	Absolute error
A_{ar}	Ash as received coal
$F_{c,ar}$	Fixed carbon as received coal
C_{ar}	Carbon content as received coal
O_{ar}	Oxygen content as received coal
S_{ar}	Sulfur content as received coal
F_G	Gaussian filtering image dataset
F_{R-CNN}	Mask R-CNN processing image dataset

References

Al-Bulqini, H. M., E. B. Zeidan, F. M. Okasha, and M. S. Mansour. 2023. An image processing technique for studying the flame structure using single shots of oh-PLIF diagnostics. *Mansoura Engineering Journal* 48 (5):5. doi:10.58491/2735-4202.3071

Ali, M. A., S. E. Najim, and Q. A. Rishack. 2017. Cfd analysis of a 200mw tangential gas fired furnace boiler. *International Journal of Engineering Research & Technology* 6 (8):184–91. doi:10.17577/IJERTV6IS080092

Belošević, S., I. Tomanović, N. Crnomarković, and A. Milićević. 2019. Full-scale cfd investigation of gas-particle flow, interactions and combustion in tangentially fired pulverized coal furnace. *Energy* 179:1036–53. doi:10.1016/j.energy.2019.05.066

Blondeau, J., J. Van den Auweele, S. Alimuddin, F. Binder, and F. Turoni. 2020. Online adjustment of furnace exit gas temperature field using advanced infrared pyrometry: Case study of a 1500 mw utility boiler. *Case Studies in Thermal Engineering* 21 (100649). doi: 10.1016/j.csite.2020.100649

Chaib, O., Y. Zheng, S. Hochgreb, and I. Boxx. 2023. Hybrid algorithm for the detection of turbulent flame fronts. *Experiments in Fluids* 64 (5). doi: 10.1007/s00348-023-03651-6

Chen, J., L. L. T. Chan, and Y. Cheng. 2013. Gaussian process regression based optimal design of combustion systems using flame images. *Applied Energy* 111:111 153–60. doi:10.1016/j.apenergy.2013.04.036

Chen, T., Y. Zhang, M. Liao, and W. Wang. 2019. Coupled modeling of combustion and hydrodynamics for a coal-fired supercritical boiler. *Fuel* 240:49–56. doi:10.1016/j.fuel.2018.11.008

He, K., G. Gkioxari, P. Dollár, and R. Girshick. 2017. Mask r-cnn. arxiv. doi:10.48550/arXiv.1703.06870

Jiang, W., T. Pan, G. Jiang, Z. Sun, H. Liu, Z. Zhou, B. Ruan, K. Yang, and X. Gao. 2023. Data-driven physical fields reconstruction of supercritical-pressure flow in regenerative cooling channel using pod-ae reduced-order model. *International Journal of Heat and Mass Transfer* 217 (124699). doi: 10.1016/j.ijheatmasstransfer.2023.124699

Kong, Q., G. Jiang, Y. Liu, and J. Sun. 2020. 3d high-quality temperature-field reconstruction method in furnace based on acoustic tomography. *Applied Thermal Engineering* 179 (115693). doi: 10.1016/j.applthermaleng.2020.115693

Lingkai, Z., and L. Li. 2020. Video flame detection method based on improved fast robust feature. *Journal of Physics Conference Series* 1518 (1):12065. doi:10.1088/1742-6596/1518/1/012065

Lou, C., and Z. Zhang. 2019. Experimental and numerical analysis of radiative entropy generation in industrial and boiler furnaces. *Journal of Quantitative Spectroscopy and Radiative Transfer* 232:27–34. doi:10.1016/j.jqsrt.2019.04.039

Lv, M., J. Zhao, S. Cao, T. Shen, and Z. Tang. 2023. Prediction of temperature distribution in a furnace using the incremental deep extreme learning machine. *PeerJ Computer Science* 9 (e1218). doi:10.7717/peerj-cs.1218

Mu, H., Z. Li, Z. Han, J. Li, H. I. Schlaberg, Shiliu, and S. Liu. 2015. Visualization measurement of the flame temperature in a power station using the colorimetric method. *Energy Procedia* 66:133–36. doi:10.1016/j.egypro.2015.02.075

Nemitallah, M. A., M. A. Nabhan, M. Alowaifeer, A. Haeruman, F. Alzahrani, M. A. Habib, M. Elshafei, M. I. Abouheaf, M. Aliyu, and M. Alfarraj. 2023. Artificial intelligence for control and optimization of boilers' performance and emissions: A review. *Journal of Cleaner Production* 417 (138109). doi: 10.1016/j.jclepro.2023.138109

Niu, C., H. Guo, and Y. Wang, "Fast flame recognition algorithm base on segmentation network," 2023 IEEE Conference on Virtual Reality and 3D User Interfaces Abstracts and Workshops (VRW), Shanghai, China, 2023, pp. 458–61, 10.1109/VRW58643.2023.00099

Petrucci, L., F. Ricci, R. Martinelli, and F. Mariani. 2022. Detecting the flame front evolution in spark-ignition engine under lean condition using the mask r-cnn approach. *Vehicles* 4 (4):978–95. doi:10.3390/vehicles4040053

Ronquillo-Lomeli, G., and A. García-Moreno. 2024. A machine learning-based approach for flames classification in industrial heavy oil-fire boilers. *Expert Systems with Applications* 238 (122188). doi:10.1016/j.eswa.2023.122188

Shi, Y., W. Zhong, X. Chen, A. B. Yu, and J. Li. 2019. Combustion optimization of ultra supercritical boiler based on artificial intelligence. *Energy* 170:804–17. doi:10.1016/j.energy.2018.12.172

Strušnik, D., M. Agrež, J. Avsec, and M. Golob. 2021. Optimisation of an old 200mw coal-fired boiler with urea injection through the use of supervised machine learning algorithms to achieve cleaner power generation. *Journal of Cleaner Production* 290 (125200). doi: 10.1016/j.jclepro.2020.125200

Sun, F., A. Huang, Z. Wu, W. Huang, and M. Zhang. 2022. A fast reconstruction method for temperature field based on principal component analysis and convolutional autoencoder. *2022 IEEE International Symposium on Product Compliance Engineering - Asia (ISPCE-ASIA)* 12:1–5. doi:10.1109/ISPCE-ASIA57917.2022.9971011

Tan, P., Q. Fang, S. Zhao, C. Yin, C. Zhang, H. Zhao, and G. Chen. 2018. Causes and mitigation of gas temperature deviation in tangentially fired tower-type boilers. *Applied Thermal Engineering* 139:135–43. doi:10.1016/j.applthermaleng.2018.04.131

Tang, Z., Y. Yang, L. Pan, M. Sui, and S. Cao. 2023. Fast prediction of heat flux distribution in boilers using computational fluid dynamics simulation data via multi-extreme learning machines. *Journal of Chemical Engineering of Japan* 56 (1). doi: 10.1080/00219592.2023.2260416

Wang, C., Y. Liu, S. Zheng, and A. Jiang. 2018. Optimizing combustion of coal fired boilers for reducing nox emission using gaussian process. *Energy* 153:149–58. doi:10.1016/j.energy.2018.01.003

Wang, Y., Y. Yu, X. Zhu, and Z. Zhang. 2020. Pattern recognition for measuring the flame stability of gas-fired combustion based on the image processing technology. *Fuel* 270 (117486). doi: 10.1016/j.fuel.2020.117486

Wu, Y., X. Zhou, L. Zhao, C. Dong, H. Wang, and B. Shotorban. 2021. A method for reconstruction of boiler combustion temperature field based on acoustic tomography. *Mathematical Problems in Engineering* 2021:1–11. doi:10.1155/2021/9922698

Xiong, W., "Research on Fire Detection and Image Information Processing System Based on Image Processing," 2020 International Conference on Advance in Ambient Computing and Intelligence (ICAACI), Ottawa, ON, Canada, 2020, pp. 106–09, 10.1109/ICAACI50733.2020.00027

Ye, T., M. Dong, Y. Liang, J. Long, W. Li, and J. Lu. 2022. Modeling and optimization of the nox generation characteristics of the coal-fired boiler based on interpretable machine learning algorithm. *International Journal of Green Energy* 19 (5):529–43. doi:10.1080/15435075.2021.1947827

Ye, T., M. Dong, Y. Liang, J. Long, Y. Zheng, and J. Lu. 2023. Online optimization of boiler operation based on information integration and case-based reasoning. *International Journal of Green Energy* 20 (1):15–27. doi:10.1080/15435075.2021.2021417

Ye, T., M. Dong, J. Long, Y. Zheng, Y. Liang, and J. Lu. 2022. Multi-objective modeling of boiler combustion based on feature fusion and bayesian optimization. *Computers & Chemical Engineering* 165 (107913). doi: 10.1016/j.compchemeng.2022.107913

Zhang, S., G. Shen, and L. An. 2019. Online monitoring of furnace exit gas temperature in power plants. *Applied Thermal Engineering* 147:917–26. doi:10.1016/j.applthermaleng.2018.11.004

Zhou, Y., C. Zhang, X. Han, and Y. Lin. 2021. Monitoring combustion instabilities of stratified swirl flames by feature extractions of time-averaged flame images using deep learning method. *Aerospace Science and Technology* 109 (106443). doi: 10.1016/j.ast.2020.106443